ENGINEERING

A multifunctional electronic skin based on patterned metal films for tactile sensing with a broad linear response range

Min Cai[1], Zhongdong Jiao[2], Shuang Nie[1], Chengjun Wang[1], Jun Zou[2,3], Jizhou Song[1,3]*

Electronic skins (e-skins) with multifunctional sensing functions have attracted a lot of attention due to their promising applications in intelligent robotics, human-machine interfaces, and wearable healthcare systems. Here, we report a multifunctional e-skin based on patterned metal films for tactile sensing of pressure and temperature with a broad linear response range by implementing the single sensing mechanism of piezoresistivity, which allows for the easy signal processing and simple device configuration. The sensing pixel features serpentine metal traces and spatially distributed microprotrusions. Experimental and numerical studies reveal the fundamental aspects of the multifunctional tactile sensing mechanism of the e-skin, which exhibits excellent flexibility and wearable conformability. The fabrication approach being compatible with the well-established microfabrication processes has enabled the scalable manufacturing of a large-scale e-skin for spatial tactile sensing in various application scenarios.

INTRODUCTION

The somatosensory system of human skin contains different types of tactile receptors, which enable humans to perceive various mechanical and thermal stimuli distinctively. Electronic skin (e-skin) that imitates human somatosensory functions allows us to realize the tactile sensing ability of human skin (e.g., strain, vibration, pressure, and temperature) with promising applications in intelligent robotics (*1*–*6*), prosthetics (*7*–*9*), human-machine interfaces (*10*–*13*), and wearable healthcare systems (*14*–*18*). An ideal e-skin should offer multifunctional sensing capability, i.e., the capability of detecting different types of stimuli simultaneously (*19*–*23*). Particularly, e-skins with the ability to detect pressure and temperature at the same time are essential for self-protection, touch recognition, and object manipulation. Attempts have been actively made to decouple the pressure and temperature by implementing heterogeneous sensing mechanisms (*20*, *24*–*28*), such as the capacitance as the temperature-insensitive intrinsic variable to measure pressure (*20*) and the pyroelectric voltage (*27*) or electrical resistance (*24*) as the pressure-insensitive intrinsic variable to measure temperature. Despite notable advances, the integration of different types of sensors may cause the design and fabrication or the data acquisition to be complex. Moreover, most existing multifunctional e-skins exhibit a narrow linear sensing range (*29*–*31*), which requires additional complex signal processing to obtain accurate tactile information and greatly limits their broad utility. Thus, manufacturing a structurally simple, multiresponsive e-skin with a broad linear response range still remains a challenge.

Here, we report a multifunctional e-skin based on patterned metal films (PMFs) as receptors for tactile sensing of pressure and temperature with a broad linear response range by implementing the single sensing mechanism of widely used piezoresistivity. The bypass of the heterogeneous sensing mechanism has enabled the easy signal processing and simple device configuration. The decoupling of pressure and temperature sensing in the sensing pixel has been achieved via the design of PMFs on a soft substrate with microprotrusions. The protrusions switch the negligible out-of-plane compression-dominated deformations in PMFs to desired appreciable bending-dominated deformations and enhance the pressure sensitivity by more than 177 times. Numerical and experimental studies have been carried out to reveal the underlying decoupled sensing mechanism and the fundamental aspects of design and operation of the sensing pixel. A multifunctional e-skin of multiple sensing pixels has been fabricated via microfabrication processes, affording abilities to integrate with skin to monitor the artery pulse and swallowing process, and enabling a flexible gripper to feel the softness and temperature of objects. The concept is compatible with the well-established microfabrication processes, which has enabled the fabrication of a large-scale multifunctional e-skin for spatial tactile sensing of pressure and temperature in various application scenarios. This type of multifunctional tactile sensing design creates a promising route for scalable manufacturing of e-skins, which is highly desired in practical applications such as wearable health monitoring and human and like robotic perception.

RESULTS

Mechanism for multifunctional sensing of pressure and temperature

PMFs with a metal layer encapsulated by polyimides (PIs) are linearly resistance sensitive to their deformations and temperature change and could be used as the receptors of e-skins to detect pressure and temperature. Figure 1A schematically shows a flexible PMF with a shape of straight strip, which can be easily fabricated by well-established microfabrication processes (see fig. S1 for details). The coupled effects of strain and temperature on the resistance change of PMFs prevent the multifunctional sensing of pressure and temperature simultaneously. To solve this problem, we adopted the design of PMFs on a soft substrate with or without microprotrusions as the pressure sensing unit (P-unit) and the temperature sensing unit (T-unit), respectively. In the P-unit (Fig. 1B), the spatially distributed microprotrusions on the PMF switch the negligible out-of-plane compression of PMFs due to pressure to the appreciable

[1]Department of Engineering Mechanics, Soft Matter Research Center, and Key Laboratory of Soft Machines and Smart Devices of Zhejiang Province, Zhejiang University, 310027 Hangzhou, China. [2]School of Mechanical Engineering, Zhejiang University, 310027 Hangzhou, China. [3]State Key Laboratory of Fluid Power and Mechatronic Systems, Zhejiang University, 310027 Hangzhou, China.
*Corresponding author. Email: jzsong@zju.edu.cn

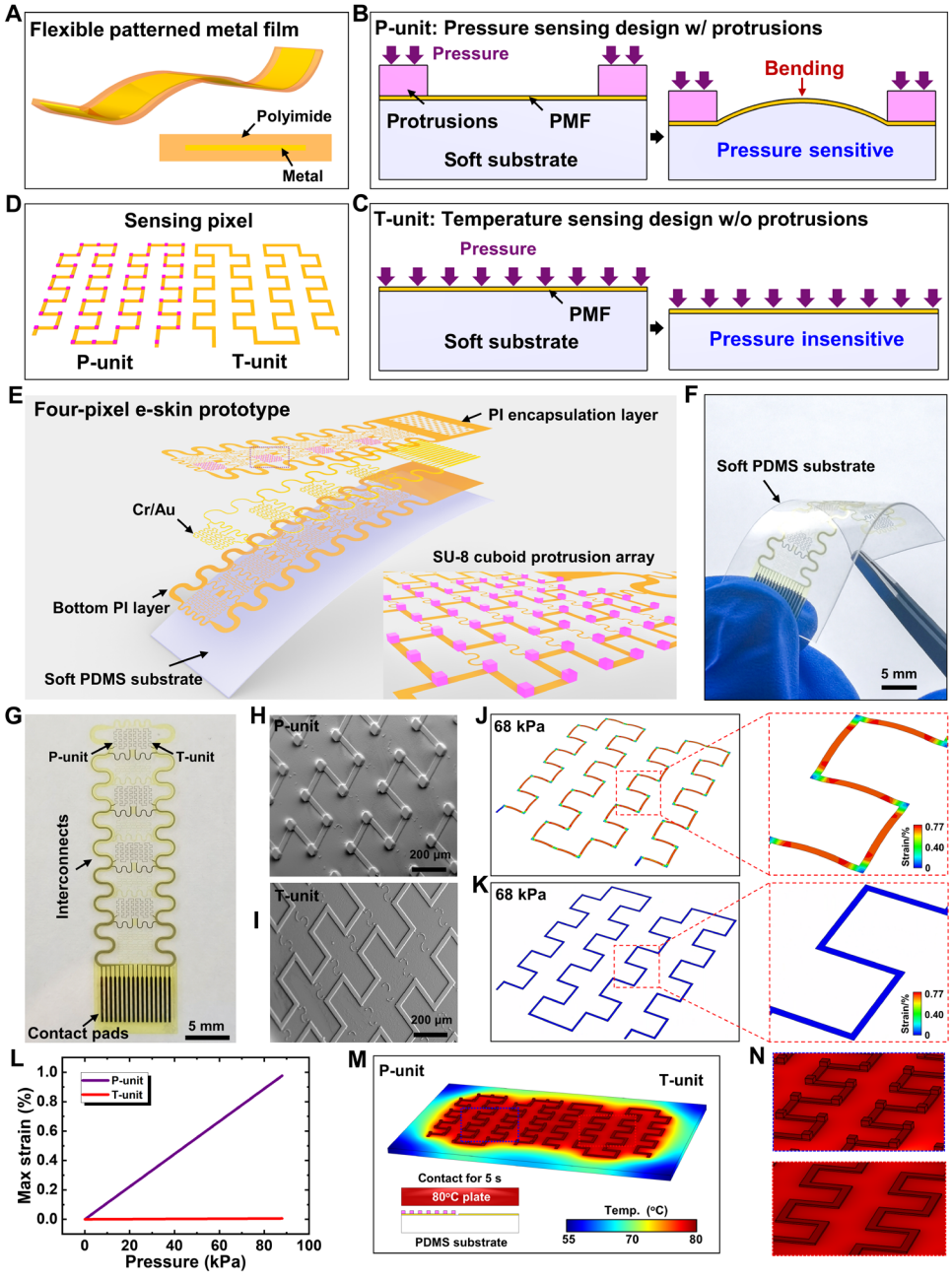

Fig. 1. The mechanism for multifunctional sensing and layout of the e-skin prototype. (**A**) Schematic of the flexible PMF with a cross-sectional view. (**B**) Schematics of the pressure-sensitive pressure sensing unit (P-unit) with microprotrusions and (**C**) the pressure-insensitive temperature sensing unit (T-unit) without microprotrusions. (**D**) Schematic of the sensing pixel constructed by combining the P-unit and T-unit with pink points denoting the protrusions. (**E** to **G**) Exploded view layout and optical images of the flexible e-skin prototype. (**H** and **I**) SEM images of the P/T-unit. (**J** and **K**) Maximum principal strain profiles in the metal layer of the P/T-unit. (**L**) Maximum principal strain in the metal layer as a function of applied pressure. (**M**) Temperature profiles of the P/T-unit with the magnified views of the P-unit (top) and the T-unit (bottom) in (**N**). PDMS, polydimethylsiloxane substrate.

bending deformation, which enables the P-unit to be pressure sensitive and leads to a measurable resistance change reflecting the magnitude of pressure. In the T-unit (Fig. 1C), the pressure induces negligible deformations in the PMF such that the T-unit is pressure insensitive; i.e., temperature could be detected by measuring the resistance change of T-unit without the interference of pressure. To improve stretchability, we both patterned the PMFs of the P/T-unit into the same stretchable serpentine shapes. A multifunctional sensing pixel can then be constructed by combining the P-unit and the T-unit (Fig. 1D). The microprotrusions (pink points in left of Fig. 1D) distributed on corners of the PMF to enhance the piezoresistive effect. When the multiple stimuli of temperature and pressure are applied on the sensing pixel, the resistance change of the P-unit is caused by both pressure and temperature, while that of the T-unit is

only caused by temperature. The resistance change of the T-unit then yields the sensing signal of temperature, which could be used to eliminate the temperature interference on the P-unit, thus yielding the accurate sensing signal of pressure (detailed illustration in note S1).

A multifunctional e-skin prototype with four sensing pixels

To demonstrate the concept of multifunctional sensing of pressure and temperature, we fabricated a flexible multifunctional e-skin with four sensing pixels by the well-established microfabrication processes. The detailed design of the flexible e-skin is shown in fig. S2, with the key fabrication process described in Materials and Methods and schematically illustrated in fig. S3. Figure 1E schematically shows the tilted exploded view layout of the flexible e-skin prototype, which consists of a soft polydimethylsiloxane substrate (PDMS; 100 μm in thickness) and eight serpentine PMF grids with a layer of metal (Cr/Au; 5/60 nm in thickness) sandwiched by the patterned PI films (5 μm in thickness) for insulation and protection. The inset of Fig. 1E is the magnified view of the selected P-unit with a discrete microprotrusion array in the cuboid shape (SU-8 photoresist; 50 μm in length, 50 μm in width, and 30 μm in height). Figure 1F shows the optical image of the flexible four-pixel e-skin prototype under bending deformation. The e-skin shows good flexibility and transparency, which allow it to adapt to different shape of surface. Figure 1G shows the device without the PDMS substrate, consisting of four sensing pixels, serpentine interconnects, and contact pads. Figure 1 (H and I) shows the scanning electron microscopy (SEM) images of the P/T-unit, respectively. The SU-8 protrusions in the P-unit naturally attach with PI firmly. As demonstrated by finite element analysis (FEA) results shown in Fig. 1 (J and K), the maximum principal strain in the metal layer of PMF of the P-unit is much larger than that of the T-unit under a given pressure of 68 kPa applied on the P/T-unit by a rigid plate (2.5 mm by 2.5 mm) (see note S2 for detailed information of FEA). The maximum principal strain in the metal layer of the T-unit for the case of pressing is 0.004%, whereas that in the metal layer of the P-unit can reach 0.77%. Figure 1L gives the maximum principal strain in the metal layer of the P/T-unit as the function of applied pressure. The huge difference indicates that the P-unit is pressure sensitive but the T-unit is pressure insensitive.

To investigate the influences of mechanical properties of substrate and geometrical structure of protrusions on the pressure sensing performance, we carried out FEA to obtain the average strain in the metal layer of the P-unit under the same applied pressure of 56 kPa, which determined the resistance change. The higher the average strain level, the better the pressure sensing performance. The strain level increases with the substrate thickness and then reaches a saturated value due to the saturated bending deformation under the given pressure when the thickness exceeds 150 μm (fig. S4A). A softer substrate induces a larger bending deformation of the P-unit and thus yields a larger strain level in the metal layer (fig. S4B). The protrusion height has a negligible effect on the average strain, since the protrusion height will not change the bending deformation of the P-unit (fig. S4C). When reducing the protrusion area (i.e., the protrusion side length), the average strain in the metal layer increases (fig. S4D). The protrusion position has a notable effect on the strain level in the metal layer, with the protrusions placing at corners of the trace much better than the middle of the straight line (figs. S4, E and F). Furthermore, as demonstrated by thermal analysis results shown in Fig. 1M, the temperature profiles of the P/T-unit are basically the same when the sensing pixels contact an 80°C plate for 5 s with the magnified views shown in Fig. 1N (see note S3 for details of thermal analysis). These FEA results have validated the multifunctional sensing functions of the e-skin by implementing the single sensing mechanism combined with the microprotrusion design.

Characterization of the multifunctional sensing performance of the e-skin

Systematic experimental studies were carried out to investigate the multifunctional sensing performance of the e-skin. Figure 2A describes the relationship between the electrical resistance variation ratio ($\Delta R/R_0$, with ΔR as the measured change in resistance and R_0 as the initial resistance without loadings) and the pressure applied on the P/T-unit. The P-unit exhibits a good linearity [coefficient of determination (R^2) = 0.995] in a broad measurable range of up to 80 kPa. Besides, the T-unit shows the insensitivity to pressure with the slope 177 times less than that of the P-unit (0.0202 and 0.000114% kPa^{-1}), which indicates that the T-unit is pressure insensitive (see Materials and Methods for details of electrical measurement). The repeatability and accuracy of the P-unit toward five different levels of pressure (139, 235, 439, 627, and 815 Pa) were shown in fig. S5. Figure 2B describes the relationship between the electrical resistance variation ratio and the temperature rise of the P/T-unit. As expected, the P/T-unit both show a good linearity and have the same thermal sensing sensitivity of 0.083% $°C^{-1}$. When the P-unit and T-unit contacted with a 43°C plate for 14 s, the real-time responses of the P-unit and T-unit were recorded and shown in Fig. 2C, which demonstrates again that the P-unit and the T-unit have the same thermal sensing performance. Figure 2D gives the dynamic response of the P-unit under a 10-kPa pressure. The response time and recovery time are 0.1 and 0.2 s, respectively, which are comparable to those in literature (*32*–*35*) and indicate that the P-unit is fast in response and recovery. Note that the object applying pressure should be larger than the distance between the protrusions. If the object is smaller than the distance between the protrusions, then the pressure sensor will not work. Considering that the distance between the protrusions is as small as 260 μm in the e-skin, it is unusual for an object to apply pressure only on the region between the protrusions.

The performance of our device was compared with other existing resistive pressure/temperature sensors with a broad linearity range of pressure detection (see table S1). Our pressure sensor outperforms most of existing resistive sensors (*32*–*34*, *36*–*38*) with regard to the linear response range, the sensitivity, and the maximum sensing range but perform comparable response/recovery time. Our temperature sensor has a similar performance with existing resistive sensors. Note that the capacitive pressure sensor could exhibit a much larger linear response range (~1 MPa) than that of this work but a much lower sensitivity with the minimum detectable pressure on the order of 10 kPa, despite that a different sensing principle is used (*39*, *40*). To evaluate the stability and robustness of the P-unit, a pressure of 10 kPa was periodically applied on the P-unit by a fatigue machine at a frequency of 3 Hz for 10,000 times (see Materials and Methods for details of fatigue test). The output of the P-unit was recorded in Fig. 2E, with the middle 20 cycles plotted in Fig. 2F. It shows that, even after the 10,000 loading/unloading cycling test, the P-unit still works well without any notable performance degradation.

The multifunctional sensing performance of the e-skin was evaluated by stimulating the sensing pixel with pressure and temperature simultaneously, as schematically shown in the inset of Fig. 2G. A

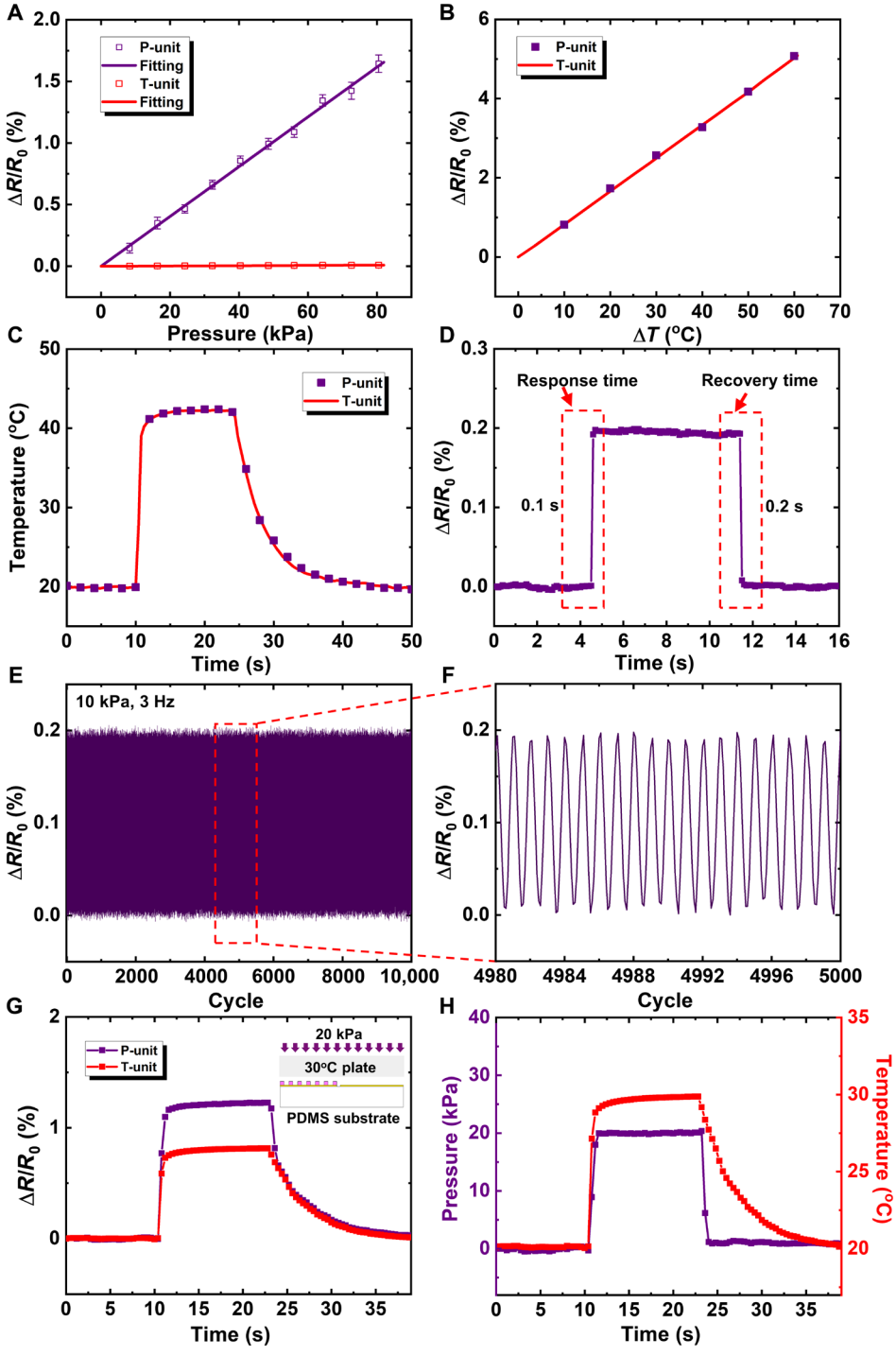

Fig. 2. Characterization of the multifunctional sensing performances. (**A**) Electrical resistance changes under various pressures applied on the P/T-unit. (**B**) Electrical resistance changes of the P/T-unit under various temperature changes. (**C**) Real-time responses to temperature change of the P/T-unit. (**D**) Dynamic response of the P-unit under a 10-kPa pressure. (**E** and **F**) Cyclic loading on the P-unit for 10,000 times at a frequency of 3 Hz. (**G**) Real-time recorded resistance changes of the P/T-unit subjected to pressing and heating simultaneously. The inset schematically shows the operation process. (**H**) The correspondingly measured pressure and temperature signal of the P-unit and the T-unit, respectively.

sensing pixel contacted to a hot plate with a surface temperature of 30°C under a pressure of 20 kPa. This experiment was carried out by a universal testing machine with a homemade loading pillar, which was integrated with a thin film heater. The electrical responses of the P/T-unit were recorded and shown in Fig. 2G. The P-unit recorded the coupled responses to temperature and pressure, while the T-unit only recorded the response to temperature. The applied pressure can then be obtained by subtracting the response of the T-unit from that of the P-unit. Figure 2H gives the measured pressure and temperature, which agree well with the actual applied external loads. These results indicate that the e-skin exhibits excellent multifunctional sensing performance.

Simultaneous monitoring of artery pulse pressure and temperature

The pulse waveform of the radial artery could be used for noninvasive and real-time diagnosis of cardiovascular problems, like diabetes, hypertension, and arteriosclerosis (*41*). The temperature of wrist skin, leading to variations in arterial stiffness and radial pressure, has a nonnegligible influence on the pulse signals (*42*, *43*). Park *et al.* (*43*) showed that the amplitude of artery pulse pressure waveform could be reduced by 70% when the wrist skin temperature changed from 20° to 42°C. Thus, to achieve the accurate collection of the pulse signals, the simultaneous measurement of artery pulse pressure and temperature is essential. With the ability to have a conformal contact to the skin, our e-skin has excellent multifunctional sensing performance and can provide high accuracy to obtain pressure and temperature, which is an ideal tool in pulse diagnosis.

Figure 3A shows the optical image of the e-skin integrated with the wrist (see fig. S6 for test details). For ease of use and accessibility, the e-skin is connected to a flexible anisotropic conductive film (ACF) cable and then integrated with a stretchable medical adhesive tape (125 μm in thickness; fig. S7). Figure 3B shows the real-time artery pressure from the top pixel of the e-skin, with the skin temperature measured as 36.2°C. The high linearity, fast response, and high accuracy of the e-skin enabled the capture of key features of the pulse waveform. Figure 3C shows the representative pulse waveform of the radial artery extracted from Fig. 3B. Valley and three typical characteristic peaks of wrist pulses were captured including the percussion wave (P wave), tidal wave (T wave), and diastolic wave (D wave), which provide important supporting information for the pulse diagnosis to quantitatively analyzing the cardiovascular parameters (*44*).

Multichannel monitoring of swallowing behavior

Dysphagia, caused by factors such as poststroke, increases the risk of lung infections, malnutrition, another stroke, and death (*45*). The real-time monitoring of swallowing process and the feedback of the curative effect have a notable impact on the establishment of the evaluation standard of swallowing function and the effective rehabilitation treatment (*46*). Thus, the accurate monitoring of swallowing process is essential and highly desired in dysphagia evaluation. However, the clinical diagnosis of swallowing is greatly limited by the expensive instruments and the experience of medical staff. These limitations can be well addressed by our e-skin with excellent sensing performance.

Figure 3D shows the optical image of the e-skin attached onto the skin of neck at the position of throat by a layer of stretchable medical adhesive tape. The four sensing pixels of the e-skin are lined up, covering the area of throat movement to monitor the pressure variations during the swallowing process. Figure 3E shows the measured pressures of four sensing pixels when having a drink of water. Before the swallowing of water, all pixels gave the same levels of initial pressure (0.4 kPa) due to the stretch of medical tape to attach the e-skin to the neck, which established the base line to measure the swallowing-induced pressure variations. The pressures of pixel 1, pixel 2, and pixel 3 increased first and then decreased to the base value, while the pressure of pixel 4 changed in an opposite way of decreasing first and then increasing to the base value. The swallowing process was completed within around 1 s. The pressure of pixel 1 gave the maximum peak value of 1.63 kPa followed by those of pixel 2 (1.38 kPa), pixel 3 (0.77 kPa), and pixel 4 (0.14 kPa). Moreover, the signal occurred first in pixel 2, with other pixels occurring later at almost the same time. Figure 3F gives spatiotemporal mapping of the swallowing process, which reflects the key features of the dynamic throat movements. These results are very useful to evaluate the swallowing function and the effectiveness of rehabilitation treatment and may provide a promising route based on a simple tool for dysphagia evaluation.

Intelligent skin of flexible gripper for tactile sensation

Robots with multifunctional tactile sensing capabilities are attractive due to their intelligent sensing abilities of self-protection, touched recognition, and objects manipulation. When the robot touches an object, the pressure and temperature are usually the most desired tactile information, since they are directly related to the feelings (i.e., soft or hard and cold or hot). Here, we fabricated a flexible gripper (fig. S8) consisting of two fingers and integrated our e-skin on the inside surface of one finger, as shown in Fig. 3G with the magnified view of the e-skin in Fig. 3H (see Materials and Methods for fabrication details). The bending deformation and the grasping pressure (or force) can be well controlled by adjusting the air pressure in the gripper. Figure 3I shows the grasping posture driven by an air pressure of 100 kPa (defined as level 3), with the finger bending inward for grasping objects. Three levels of air pressure were chosen to drive the flexible gripper to grasp an empty glass with the tactile pressure recorded, as shown in Fig. 3J and its inset (only the response of pixel 2 were given as a representative). The tactile pressures corresponding to the three levels of air pressure were 1.9, 7.6, and 12.8 kPa, respectively. Note that the deformation of flexible gripper had a negligible effect on the signal of the sensor, since only 0.004% resistance change was induced under the air pressure of 100 kPa, which is much smaller than that caused by touching (0.26% resistance change). Therefore, the signal variation of the e-skin only reflected the tactile pressure.

The ability of the intelligent skin on the flexible gripper to detect the softness of objects was demonstrated by grasping the sponge and steel ball made of different materials with the same diameter of 63 mm, as illustrated in Fig. 3 (K and L). When the flexible gripper, driven by the same air pressure of level 2, held the balls for 5.5 s, the resulted tactile pressures at the pixel 2 were recorded in Fig. 3M, with the magnitude reflecting the relative softness of the balls. The softer the ball, the lower the tactile pressure. The tactile pressure of the sponge ball (6.22 kPa) is significantly less than the steel ball (7.64 kPa), which indicates that the sponge ball is much softer than the steel ball. To quantify the softness of objects, we required an additional calibration test. Besides the softness of objects, the tactile pressure profile on the three-dimensional (3D) surface can also be obtained, as illustrated in Fig. 3N, which may provide additional information of the surface morphology of object.

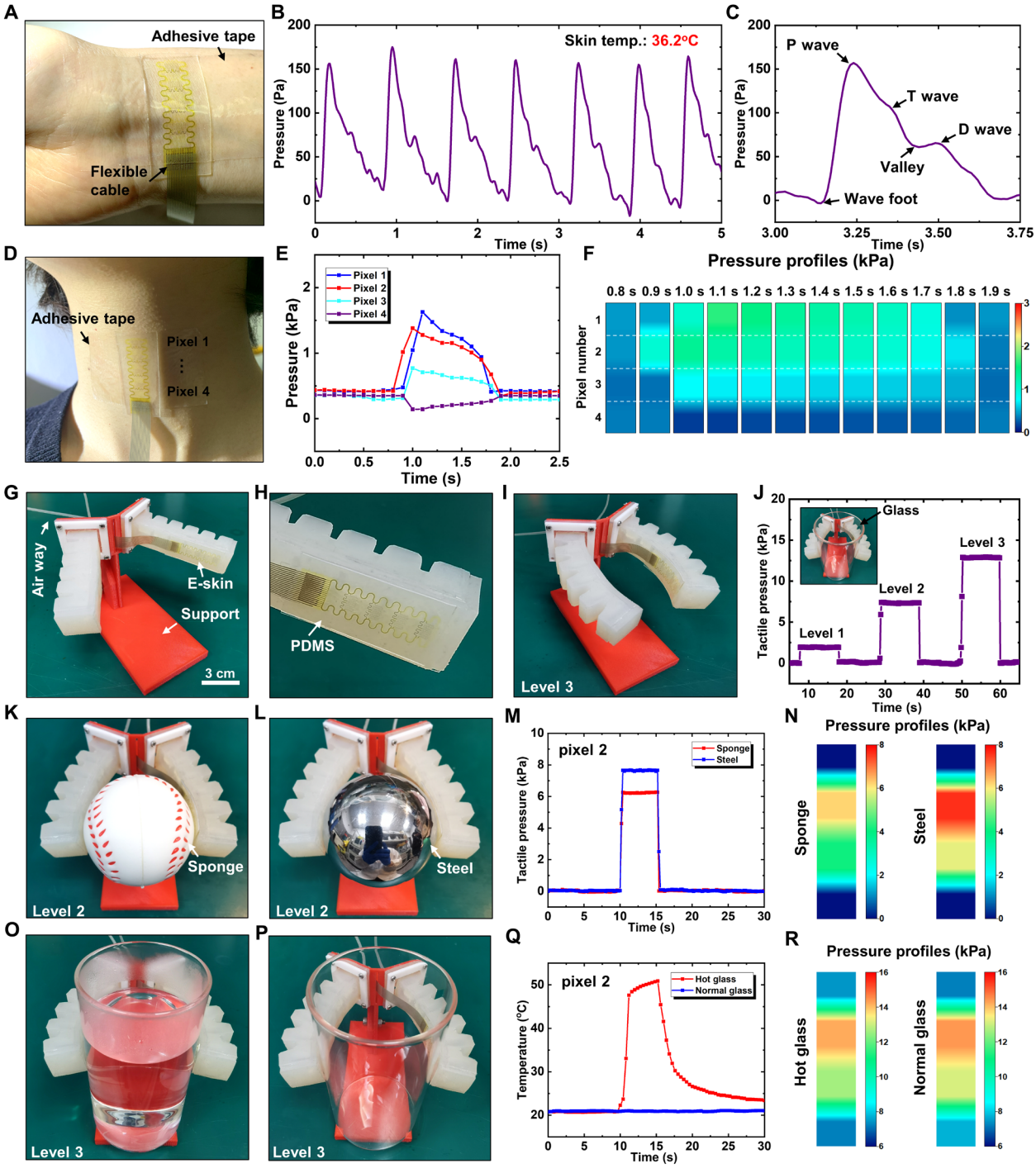

Fig. 3. Biological and intelligent applications of the e-skin prototype for sensing of pressure and temperature. (**A**) Optical image of the e-skin mounted onto the wrist. (**B**) Real-time artery pressure measured by the e-skin. (**C**) Representative pulse waveform of the radial artery extracted from (B). (**D**) Optical image of the e-skin mounted onto the neck at the position of throat. (**E**) Measured pressures of four sensing pixels when having a drink of water. (**F**) Spatiotemporal mapping of the swallowing process. (**G**) Optical image of the flexible gripper with one finger integrated with the e-skin on the inside surface (**H**). (**I**) Grasping posture driven by an air pressure of 100 kPa (level 3). (**J**) The tactile pressure recorded by pixel 2 when grasping an empty glass driven by three levels of air pressure (50, 75, and 100 kPa). (**K** and **L**) Optical images of grasping the sponge and steel balls, respectively. (**M** and **N**) Tactile pressure recorded by pixel 2 of the e-skin and tactile pressure profiles when grasping the sponge and steel ball. (**O** and **P**) Optical images of grasping glasses with or without hot water, respectively. (**Q** and **R**) Tactile temperature at pixel 2 and tactile pressure profiles when grasping glasses with or without hot water. Photo credit: M. Cai, Zhejiang University.

The ability of the intelligent skin on the flexible gripper to detect the temperature of objects was demonstrated by grasping glasses with or without hot water, as illustrated in Fig. 3 (O and P). The resulted tactile temperatures at the pixel 2 were recorded by holding the glasses for 5.5 s in Fig. 3Q, which indicates that our e-skin has the potential for self-protection of gripper from high temperature when combined with a feedback control mechanism. Besides the temperature of objects, the tactile pressure profile on the glasses can also be obtained, as illustrated in Fig. 3R. Since the glasses have the same surface morphology, the resulted tactile pressures are same for the cases with or without hot water.

Flexible large-scale e-skins for spatial sensing of pressure and temperature

The design and fabrication of the flexible e-skin prototype with four sensing pixels are compatible with the well-established microfabrication processes such that the development of a large-scale e-skin is possible for spatial sensing of pressure and temperature. To demonstrate the

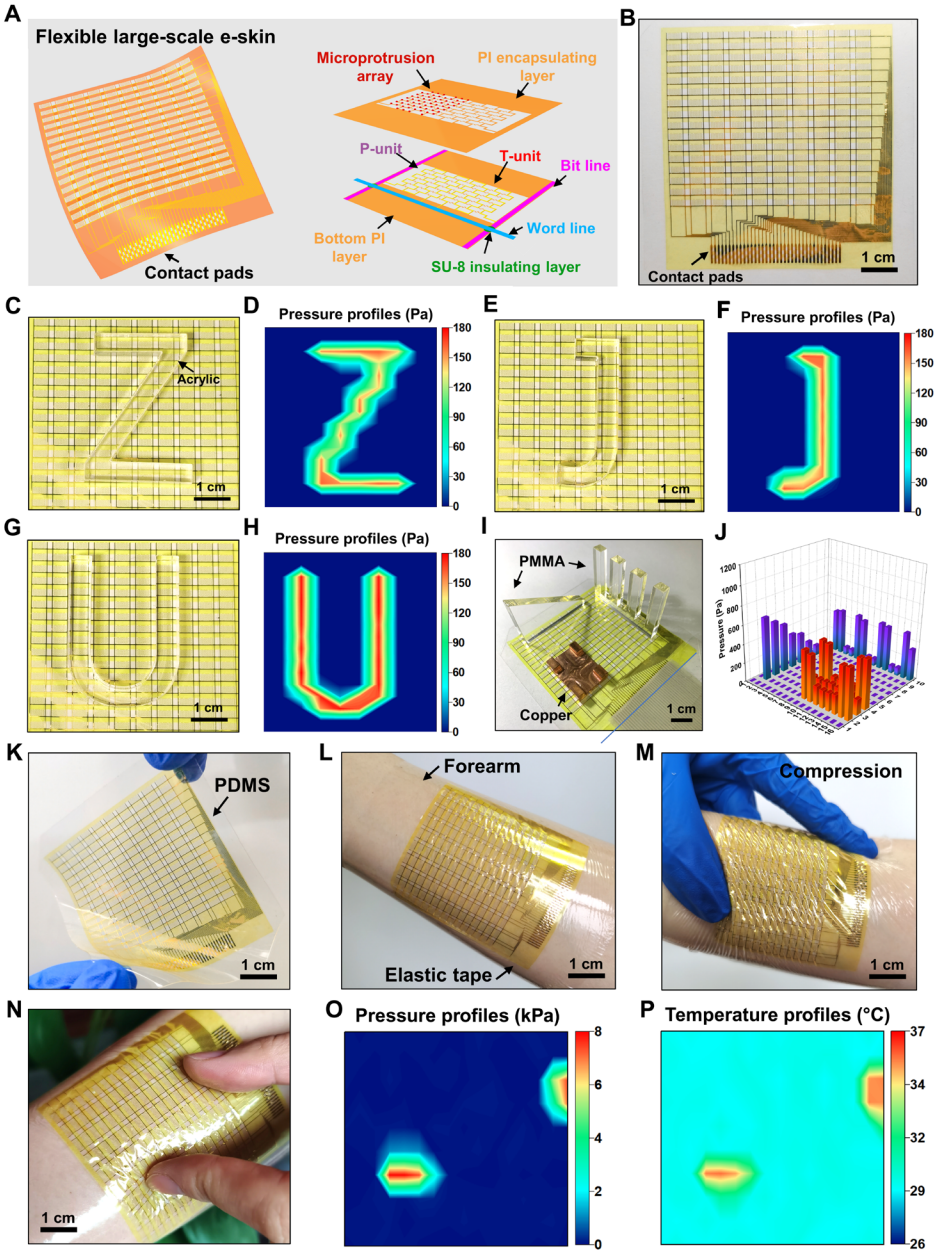

Fig. 4. Flexible large-scale e-skins for spatial sensing of pressure and temperature. (**A**) Schematic of the flexible large-scale e-skin with the exploded view of one single sensing pixel. (**B**) Optical image of the flexible large-scale e-skin. (**C**, **E**, and **G**) Optical images of the flexible large-scale e-skin with a Z-shaped, a J-shaped, and a U-shaped acrylic block on it, respectively. (**D**, **F**, and **H**) The corresponding pressure profiles measured by the e-skin. (**I**) Optical image of the flexible large-scale e-skin with different objects placed on it. (**J**) 3D bar charts of pressure distribution corresponding to (I). (**K**) Optical image of the deformed flexible large-scale e-skin with a PDMS substrate. (**L** and **M**) Optical images of the flexible large-scale e-skin mounted onto the forearm in a conformal form and under compression. (**N**) Optical images of the e-skin mounted onto the forearm pressed by two fingers. (**O** and **P**) The pressure and temperature profiles given by the e-skin. Photo credit: M. Cai, Zhejiang University.

scalability of design, we fabricated a flexible large-scale e-skin consisting of 16 × 10 sensing pixels. Figure 4A schematically shows the overall structure of the flexible large-scale e-skin with the exploded view of one single sensing pixel, which consists of the P-unit and T-unit, bottom PI layer, SU-8 insulating layers, PI encapsulating layer, and microprotrusion array as well as the word and bit interconnects (see Materials and Methods for the key fabrication process). The optical image of the fabricated flexible large-scale e-skin is shown in Fig. 4B, which covers an in-plane size of 6.2 cm by 6.6 cm. The area of each of the pixel is approximately 4 × 2.1 mm^2. The detailed design of the flexible large-scale e-skins is shown in fig. S9, with the key fabrication process described in Materials and Methods and schematically illustrated in fig. S10. A homemade circuit based on the virtual ground method (*47*, *48*) was used to readout the resistive sensors array with all of the row or column nodes placed at virtually equal potential by using the virtual ground of high-gain operational amplifiers (LM358) in the negative feedback.

Figure 4 (C, E, and G) shows the optical images of the flexible large-scale e-skin with a Z-shaped (7.4 g), a J-shaped (4.4 g), and a U-shaped (8.1 g) acrylic block on it, respectively. The corresponding measured pressure distributions by the e-skin are given in Fig. 4 (D, F, and H), which indicates that the spatial pressure variations due to slight weight objects can be recognized. In addition, objects of different materials and thicknesses were selected and placed on the e-skin, as shown in Fig. 4I, including a crenel-shaped acrylic block, a wedge-shaped acrylic block, and a copper mini table. The resulted pressure distribution is presented as 3D bar charts for better digitally reconstruct the shape of object in Fig. 4J. Furthermore, the flexible large-scale e-skin integrated with a layer of PDMS (100 μm thickness) shows an extraordinary flexibility in Fig. 4K. This flexible large-scale e-skin was mounted onto the forearm in a conformal form by a layer of stretchable adhesive tape and deformed with the skin even under a large mechanical compression of the skin, as shown in Fig. 4 (L and M). Figure 4N shows the two fingers pressed on the e-skin, and the contact points were identified by measuring the pressure and temperature on a reconstructed map, as shown in Fig. 4 (O and P, respectively).

DISCUSSION

In summary, we present a multifunctional e-skin based on PMFs for tactile sensing of pressure and temperature change with a broad linear response range of 80 kPa and 60°C. The decoupling of pressure and temperature sensing in the sensing pixel has been achieved via the design of PMFs on a soft substrate with microprotrusions. The e-skin has excellent mechanical flexibility, easy processing ability, and simple device configuration. Demonstrations of the multifunctional e-skin on skin to monitor the artery pulse and swallowing process and flexible gripper to feel softness and temperature of objects illustrate its robust capabilities. The design methodology and fabrication approach are fully compatible with well-established microfabrication processes, which enable the scalable manufacturing of a large-scale flexible multifunctional e-skin with 16 × 10 sensing pixels for spatial tactile sensing of pressure and temperature in various application scenarios. The results reported here provide an important foundation for the construction of multifunctional e-skin and create engineering opportunities for applications such as wearable health monitoring and human-like robotic perception.

MATERIALS AND METHODS

Fabrication of the four-pixel e-skin prototype

To fabricate the four-pixel e-skin prototype, a glass substrate was cleaned and then baked at 120°C for 15 min on a hotplate for dehydration. The PI precursor solution (ZKPI-305IIE, POME) was spin-coated [4000 revolutions per minute (rpm) for 60 s, 2.5 μm] on the substrate, followed by curing at 230°C for 2.5 hours. The serpentine metal layer (Cr/Au; 5/60 nm) was patterned on the PI through photolithography and electron beam evaporation (DZS-500, SKY). Another PI layer as encapsulation was spin-coated (4000 rpm for 60 s, 2.5 μm) on it and patterned by an inductively coupled plasma etching (ICP-100A, TAILONG). The SU-8 (GM1060, Gersteltec) was spin-coated (2500 rpm for 40 s, 30 μm) on it and patterned photolithography to form spatially distributed microprotrusions. The four-pixel e-skin was then released in the buffer oxidation etching (BOE) solution (RESEMI) and picked up by a water-soluble tape (ASW-1, AQUASOL) exposed on its underside for deposition of a thin layer of Cr/SiO_2 (5/30 nm) by electron beam evaporation. The four-pixel e-skin was transferred onto a PDMS substrate with its surface activated by ozone. Last, the water-soluble tape was dissolved in water, and a flexible ACF cable was thermally (150°C for 30 s) bonded to the contact pads of the four-pixel e-skin prototype at one side and to the external data acquisition circuit at the other side.

Electrical measurement of the sensing performance of the e-skin

The e-skin was connected to the electrical signal recording equipment by a flexible ACF cable. The electrical resistance of sensing pixel was recorded by a digital multimeter (34470A, Keysight) or a voltage acquisition card (HRF USB-4626). The digital multimeter was used for the resistance recording of a single P-unit or T-unit, and the voltage acquisition card was used for the multichannel recording.

Fatigue test of the P-unit

Fatigue tests were carried out by a fatigue testing system (M-100, CARE Measurement & Control) with a loading pillar (2.5 mm in width and 2.5 mm in length). The compression force was selected as 62.5 mN, which was applied on the P-unit to generate a pressure of 10 kPa. The fatigue cycling was carried out under the sinusoidal force control at a loading frequency of 3 Hz and an amplitude of 62.5 mN. Meanwhile, the e-skin was connected to the digital multimeter for electrical measurement.

Fabrication of the flexible gripper

The fabrication of the flexible gripper began with the 3D printing of a removable mold. Silicone rubber (E630, Hongyejie) was prepared with the *A*/*B* components mass ratio of 1:1, poured into the mold, and followed by baking at 65°C for 0.5 hours in an oven. After removing the mold, the resulted tubes were connected with the chamber of flexible gripper at one side and to the external pneumatic pressure device at the other side for motion control. Last, a support was 3D printed for mounting the flexible gripper.

Fabrication of the flexible large-scale e-skin

To fabricate the flexible large-scale e-skin, a glass substrate was cleaned and then baked at 120°C for 15 min on a hotplate for dehydration. The PI precursor solution (ZKPI-305IIE, POME) was spin-coated (4000 rpm for 60 s, 2.5 μm) on the substrate, followed by curing at 230°C for 2.5 hours. The serpentine metal layer (Cr/Au;

5/60 nm) was patterned on the PI through photolithography and electron beam evaporation, followed by depositing a patterned bit line (Cr/Au; 5/150 nm). A layer of SU-8 (GM 1040, Gersteltec) was spin-coated (1600 rpm for 40 s, 2 μm) and patterned photolithography for insulation. The word line (Cr/Au; 5/150 nm) was then deposited and patterned on it. Another PI layer as encapsulation was spin-coated (4000 rpm for 60 s, 2.5 μm) on it and patterned by an inductively coupled plasma etching with Al as the mask. After dissolved the Al mask, a layer of SU-8 (GM 1060, Gersteltec) was spin-coated (2500 rpm for 40 s, 30 μm) on it and patterned photolithography to form spatially distributed microprotrusions. The flexible large-scale e-skin was then released in BOE and picked up by a water-soluble tape exposed on its underside for deposition of a thin layer of Cr/SiO_2 (5/30 nm) by electron beam evaporation. The flexible large-scale e-skin was transferred to a PDMS substrate (100 μm in thickness) with its surface activated by ozone. Last, the water-soluble tape was dissolved in water, and a flexible ACF cable was thermally (150°C for 30 s) boned to the contact pads of the flexible large-scale e-skin at one side and to the external data acquisition circuit at the other side. With the aid of a layer of stretchable adhesive tape, the flexible large-scale e-skin could be mounted on the forearm.

Research standards

Statement of experiments on human skin

All experiments on human skin were approved by the Human Research Ethics Committee of Zhejiang University. Informed consent was obtained from all participants.

SUPPLEMENTARY MATERIALS

Supplementary material for this article is available at https://science.org/doi/10.1126/sciadv.abl8313

REFERENCES AND NOTES

1. B. Shih, D. Shah, J. Li, T. G. Thuruthel, Y. L. Park, F. Iida, Z. Bao, R. Kramer-Bottiglio, M. T. Tolley, Electronic skins and machine learning for intelligent soft robots. *Sci. Robot.* **5**, eaaz9239 (2020).
2. G. Yao, L. Xu, X. Chen, Y. Li, X. Huang, W. Guo, S. Liu, Z. Wang, H. Wu, Bioinspired triboelectric nanogenerators as self-powered electronic skin for robotic tactile sensing. *Adv. Funct. Mater.* **30**, 1907312 (2020).
3. J. Byun, Y. Lee, J. Yoon, B. Lee, E. Oh, S. Chung, T. Lee, K. J. Cho, J. Kim, Y. Hong, Electronic skins for soft, compact, reversible assembly of wirelessly activated fully soft robots. *Sci. Robot.* **3**, eaas9020 (2018).
4. C. M. Boutry, M. Negre, M. Jorda, O. Vardoulis, A. Chortos, O. Khatib, Z. Bao, A hierarchically patterned, bioinspired e-skin able to detect the direction of applied pressure for robotics. *Sci. Robot.* **3**, eaau6914 (2018).
5. B. C. K. Tee, C. Wang, R. Allen, Z. Bao, An electrically and mechanically self-healing composite with pressure- and flexion-sensitive properties for electronic skin applications. *Nat. Nanotechnol.* **7**, 825–832 (2012).
6. X. Cheng, Z. Liu, T. Jin, F. Zhang, H. Zhang, Y. Zhang, Bioinspired design and assembly of a multilayer cage-shaped sensor capable of multistage load bearing and collapse prevention. *Nanotechnology* **32**, 155506 (2021).
7. J. Yang, J. Mun, S. Y. Kwon, S. Park, Z. Bao, S. Park, Electronic skin: Recent progress and future prospects for skin-attachable devices for health monitoring, robotics, and prosthetics. *Adv. Mater.* **31**, 1904765 (2019).
8. Z. Liang, J. Cheng, Q. Zhao, X. Zhao, Z. Han, Y. Chen, Y. Ma, X. Feng, High-performance flexible tactile sensor enabling intelligent haptic perception for a soft prosthetic hand. *Adv. Mater. Technol.* **4**, 1900317 (2019).
9. P. Li, H. P. A. Ali, W. Cheng, J. Yang, B. C. K. Tee, Bioinspired prosthetic interfaces. *Adv. Mater. Technol.* **5**, 1900856 (2020).
10. Y. Yu, J. Nassar, C. Xu, J. Min, Y. Yang, A. Dai, R. Doshi, A. Huang, Y. Song, R. Gehlhar, A. D. Ames, Biofuel-powered soft electronic skin with multiplexed and wireless sensing for human-machine interfaces. *Sci. Robot.* **5**, eaaz7946 (2020).
11. T. An, D. V. Anaya, S. Gong, L. W. Yap, F. Lin, R. Wang, M. R. Yuce, W. Cheng, Self-powered gold nanowire tattoo triboelectric sensors for soft wearable human-machine interface. *Nano Energy* **77**, 105295 (2020).
12. S. Wang, J. Xu, W. Wang, G. J. N. Wang, R. Rastak, F. Molina-Lopez, J. W. Chung, S. Niu, V. R. Feig, J. Lopez, T. Lei, S. K. Kwon, Y. Kim, A. M. Foudeh, J. B. H. Tok, Z. Bao, Skin electronics from scalable fabrication of an intrinsically stretchable transistor array. *Nature* **555**, 83–88 (2018).
13. F. M. Ferrari, U. Ismailov, J.-M. Badier, F. Greco, E. Ismailova, Conducting polymer tattoo electrodes in clinical electro- and magneto-encephalography. *npj Flex. Electron.* **4**, 4 (2020).
14. X. Wang, Y. Gu, Z. Xiong, Z. Cui, T. Zhang, Silk-molded flexible, ultrasensitive, and highly stable electronic skin for monitoring human physiological signals. *Adv. Mater.* **26**, 1336–1342 (2014).
15. Z. Ma, S. Li, H. Wang, W. Cheng, Y. Li, L. Pan, Y. Shi, Advanced electronic skin devices for healthcare applications. *J. Mater. Chem. B* **7**, 173–197 (2019).
16. G. Liu, L. Sun, Y. Su, Scaling effects in the mechanical system of the flexible epidermal electronics and the human skin. *ASME J. Appl. Mech.* **87**, 081007 (2020).
17. H. Li, Y. Ma, Z. Liang, Z. Wang, Y. Cao, Y. Xu, H. Zhou, B. Lu, Y. Chen, Z. Han, S. Cai, X. Feng, Wearable skin-like optoelectronic systems with suppression of motion artifacts for cuff-less continuous blood pressure monitor. *Natl. Sci. Rev.* **7**, 849–862 (2020).
18. H. Li, H. Liu, M. Sun, Y. Huang, L. Xu, 3D interfacing between soft electronic tools and complex biological tissues. *Adv. Mater.* **33**, 2004425 (2020).
19. F. Zhang, Y. Zang, D. Huang, C. A. Di, D. Zhu, Flexible and self-powered temperature-pressure dual-parameter sensors using microstructure-frame-supported organic thermoelectric materials. *Nat. Commun.* **6**, 8356 (2015).
20. Q. Hua, J. Sun, H. Liu, R. Bao, R. Yu, J. Zhai, C. Pan, Z. Wang, Skin-inspired highly stretchable and conformable matrix networks for multifunctional sensing. *Nat. Commun.* **9**, 244 (2018).
21. I. You, D. G. Mackanic, N. Matsuhisa, J. Kang, J. Kwon, L. Beker, J. Mun, W. Suh, T. Y. Kim, J. B. H. Tok, Z. Bao, U. Jeong, Artificial multimodal receptors based on ion relaxation dynamics. *Science* **370**, 961–965 (2020).
22. K. Xu, Y. Lu, K. Takei, Multifunctional skin-inspired flexible sensor systems for wearable electronics. *Adv. Mater. Technol.* **4**, 1800628 (2019).
23. Y. Ma, Y. Zhang, S. Cai, Z. Han, X. Liu, F. Wang, Y. Cao, Z. Wang, H. Li, Y. Chen, X. Feng, Flexible hybrid electronics for digital healthcare. *Adv. Mater.* **32**, 1902062 (2020).
24. G. Y. Bae, J. T. Han, G. Lee, S. Lee, S. W. Kim, S. Park, J. Kwon, S. Jung, K. Cho, Pressure/temperature sensing bimodal electronic skin with stimulus discriminability and linear sensitivity. *Adv. Mater.* **30**, 1803388 (2018).
25. S. Zhao, R. Zhu, Electronic skin with multifunction sensors based on thermosensation. *Adv. Mater.* **29**, 1606151 (2017).
26. J. O. Kim, S. Y. Kwon, Y. Kim, H. B. Choi, J. Yang, J. Oh, H. S. Lee, J. Y. Sim, S. Ryu, S. Park, Highly ordered 3d microstructure-based electronic skin capable of differentiating pressure, temperature, and proximity. *ACS Appl. Mater. Interfaces* **11**, 1503–1511 (2019).
27. N. T. Tien, S. Jeon, D. I. Kim, T. Q. Trung, M. Jang, B. U. Hwang, K. E. Byun, J. Bae, E. Lee, J. B. H. Tok, Z. Bao, N. E. Lee, J. J. Park, A flexible bimodal sensor array for simultaneous sensing of pressure and temperature. *Adv. Mater.* **26**, 796–804 (2014).
28. K. Sanderson, Electronic skin: From flexibility to a sense of touch. *Nature* **591**, 685–687 (2021).
29. Y. Wang, H. Wu, L. Xu, H. Zhang, Y. Yang, Z. Wang, Hierarchically patterned self-powered sensors for multifunctional tactile sensing. *Sci. Adv.* **6**, eabb9083 (2020).
30. L. Zhu, Y. Wang, D. Mei, W. Ding, C. Jiang, Y. Lu, Fully elastomeric fingerprint-shaped electronic skin based on tunable patterned graphene/silver nanocomposites. *ACS Appl. Mater. Interfaces* **12**, 31725–31737 (2020).
31. M. Khatib, O. Zohar, W. Saliba, H. Haick, A multifunctional electronic skin empowered with damage mapping and autonomic acceleration of self-healing in designated locations. *Adv. Mater.* **32**, 2000246 (2020).
32. J. Park, Y. Lee, J. Hong, M. Ha, Y. D. Jung, H. Lim, S. Y. Kim, H. Ko, Giant tunneling piezoresistance of composite elastomers with interlocked microdome arrays for ultrasensitive and multimodal electronic skins. *ACS Nano* **8**, 4689–4697 (2014).
33. Y. Pang, K. Zhang, Z. Yang, S. Jiang, Z. Ju, Y. Li, X. Wang, D. Wang, M. Jian, Y. Zhang, R. Liang, H. Tian, Y. Yang, T. L. Ren, Epidermis microstructure inspired graphene pressure sensor with random distributed spinosum for high sensitivity and large linearity. *ACS Nano* **12**, 2346–2354 (2018).
34. S. Feng, Q. Li, S. Wang, B. Wang, Y. Hou, T. Zhang, Tunable dual temperature-pressure sensing and parameter self-separating based on ionic hydrogel via multisynergistic network design. *ACS Appl. Mater. Interfaces* **11**, 21049–21057 (2019).
35. S. Yoon, J. K. Sim, Y. H. Cho, A flexible and wearable human stress monitoring patch. *Sci. Rep.* **6**, 23468 (2016).
36. H. B. Yao, J. Ge, C. F. Wang, X. Wang, W. Hu, Z. J. Zheng, Y. Ni, S. H. Yu, A flexible and highly pressure-sensitive graphene-polyurethane sponge based on fractured microstructure design. *Adv. Mater.* **25**, 6692–6698 (2013).
37. H. Dong, L. Zhang, T. Wu, H. Song, J. Luo, F. Huang, C. Zuo, Flexible pressure sensor with high sensitivity and fast response for electronic skin using near-field electrohydrodynamic direct writing. *Org. Electron.* **89**, 106044 (2021).

38. S. Han, J. Kim, S. M. Won, Y. Ma, D. Kang, Z. Xie, K. T. Lee, H. U. Chung, A. Banks, S. Min, S. Y. Heo, C. R. Davies, J. W. Lee, C. H. Lee, B. H. Kim, K. Li, Y. Zhou, C. Wei, X. Feng, Y. Huang, J. A. Rogers, Battery-free, wireless sensors for full-body pressure and temperature mapping. *Sci. Transl. Med.* **10**, eaan4950 (2018).
39. D. Lipomi, M. Vosgueritchian, B. C. K. Tee, S. L. Hellstrom, J. A. Lee, C. H. Fox, Z. Bao, Skin-like pressure and strain sensors based on transparent elastic films of carbon nanotubes. *Nat. Nanotechnol.* **6**, 788–792 (2011).
40. S. J. Woo, J. H. Kong, D. G. Kim, J. M. Kim, A thin all-elastomeric capacitive pressure sensor array based on micro-contact printed elastic conductors. *J. Mater. Chem. C* **2**, 4415–4422 (2014).
41. J. N. Cohn, S. Finkelstein, G. Mcveigh, D. Morgan, L. Lemay, J. Robinson, J. Mock, Noninvasive pulse wave analysis for the early detection of vascular disease. *Hypertension* **26**, 503–508 (1995).
42. W. B. White, L. Wolfson, D. B. Wakefield, C. B. Hall, P. Campbell, N. Moscufo, J. Schmidt, R. F. Kaplan, G. Pearlson, C. R. Guttmann, Average daily blood pressure, not office blood pressure, is associated with progression of cerebrovascular disease and cognitive decline in older people. *Circulation* **124**, 2312–2319 (2011).
43. J. Park, M. Kim, Y. Lee, H. S. Lee, H. Ko, Fingertip skin-inspired microstructured ferroelectric skins discriminate static/dynamic pressure and temperature stimuli. *Sci. Adv.* **1**, e1500661 (2015).
44. W. W. Nichols, Clinical measurement of arterial stiffness obtained from noninvasive pressure waveforms. *Am. J. Hypertens.* **18**, 3S–10S (2005).
45. D. L. Cohen, C. Roffe, J. Beavan, B. Blackett, C. A. Fairfield, S. Hamdy, D. Havard, M. McFarlane, C. McLauglin, M. Randall, K. Robson, P. Scutt, C. Smith, D. Smithard, N. Sprigg, A. Warusevitane, C. Watkins, L. Woodhouse, P. M. Bath, Post-stroke dysphagia: A review and design considerations for future trials. *Int. J. Stroke* **11**, 399–411 (2016).
46. C. D. Lind, Dysphagia: Evaluation and treatment. *Gastroenterol. Clin. N. Am.* **32**, 553–575 (2003).
47. R. S. Saxena, R. K. Bhan, A. Aggrawal, A new discrete circuit for readout of resistive sensor arrays. *Sens. Actuators A Phys.* **149**, 93–99 (2009).
48. R. S. Saxena, R. K. Bhan, N. K. Saini, R. Muralidharan, Virtual ground technique for crosstalk suppression in networked resistive sensors. *IEEE Sensors J.* **11**, 432–433 (2011).

Acknowledgments
Funding: The authors acknowledge the supports from the National Natural Science Foundation of China (grant nos. 11872331 and U20A6001) and Zhejiang University K.P. Chao's High Technology Development Foundation. **Author contributions:** M.C. and J.S. conceived the study and co-wrote the manuscript. J.S. and J.Z. supervised the project. M.C, Z.J., S.N., and J.S. planned and performed the experiments and collected and analyzed the data. C.W. assisted with the experiments. All authors discussed the results and commented on the manuscript. **Competing interests:** The authors declare that they have no competing interests. **Data and materials availability:** All data needed to evaluate the conclusions in the paper are present in the paper and/or the Supplementary Materials.

Submitted 9 August 2021
Accepted 3 November 2021
Published 22 December 2021
10.1126/sciadv.abl8313